Title
Time-lapse crosswell seismic and VSP monitoring of injected CO2 in a brine aquifer

Authors
Daley, Thomas M.
Myer, Larry R.
Peterson, J.E.
et al.

Publication Date
2006-05-30

Peer reviewed

Time-lapse crosswell seismic and VSP monitoring of injected CO_2 in a brine aquifer

Thomas M Daley*, Larry R. Myer, J.E. Peterson, E.L. Majer, G.M. Hoversten

all at Lawrence Berkeley National Laboratory, 1 Cyclotron Rd., Berkeley, Ca., 94720, USA

*tmdaley@lbl.gov

(Submitted to Environmental Geology, May 2006, revised Nov 2006)

Keywords: CO_2, sequestration, VSP, crosswell, seismic

Abstract

Seismic surveys successfully imaged a small scale CO_2 injection (1600 tons) conducted in a brine aquifer of the Frio Formation near Houston, Texas. These time-lapse bore-hole seismic surveys, crosswell and vertical seismic profile (VSP), were acquired to monitor the CO_2 distribution using two boreholes (the new injection well and a pre-existing well used for monitoring) which are 30 m apart at a depth of 1500 m. The crosswell survey provided a high-resolution image of the CO_2 distribution between the wells via tomographic imaging of the P-wave velocity decrease (up to 500 m/s). The simultaneously acquired S-wave tomography showed little change in S-wave velocity, as expected for fluid substitution. A rock physics model was used to estimate CO_2 saturations of 10-20% from the P-wave velocity change. The VSP survey resolved a large (~70%) change in reflection amplitude for the Frio horizon. This CO_2 induced reflection amplitude change allowed estimation of the CO_2 extent beyond the monitor well and on

3 azimuths. The VSP result is compared with numerical modeling of CO_2 saturations and is seismically modeled using the velocity change estimated in the crosswell survey.

Introduction

The geologic storage of CO_2 emitted from fixed sources, such as coal or gas power plants, is currently considered one of the prime technologies for short term (~ 50 year) mitigation of greenhouse gas emissions (Pacala and Socolow, 2004). Saline aquifers are generally considered a prime candidate for large scale storage. Initial studies have shown that time-lapse borehole and surface seismic surveys can be used to estimated the location of injected CO_2 in brine aquifers as well as in oil and gas reservoirs (Arts et al. 2002; Hoversten et al. 2003; Gritto et al. 2004; Xue et al. 2005). Monitoring of injected CO_2 will likely be a necessary component of any long term storage program. Therefore, understanding the seismic response of saline aquifers to injected CO_2 is an important goal.

As part of a U.S. Department of Energy (DOE) funded project on geologic sequestration of CO_2, we acquired borehole seismic surveys before and after injection of about 1600 tons of CO_2 into a saline aquifer. These time-lapse surveys consisted of crosswell and vertical seismic profile (VSP) experiments. These experiments were part of an integrated suite of scientific studies with many contributing institutions including the Texas Bureau of Economic Geology who performed the site selection process (Hovorka et al. 2006).

The VSP and crosswell are intermediate scale (1 - 100's m) geophysical surveys providing information in-between the large scale of surface seismic (km's) and the smaller scale of well logs and core measurements (mm to m). As such, they are useful tools for monitoring small scale injections and for understanding larger scale surface measurements. A summary of the VSP method and its uses is given in Balch and Lee (1984) and the crosswell method is described in Hardage (2000).

VSP and crosswell use different acquisition geometries, have different capabilities and are typically used for different goals. Figure 1a shows the VSP geometry has a surface source and borehole sensors recording direct and reflected energy. VSP data typically has higher resolution (about 10 - 30 m) than surface seismic (30 - 100 m) because the sensors are below the near surface, which is highly attenuative. Since VSP allows measurement of upgoing (reflected) and downgoing (direct) waves within the borehole depth range, it improves the tie of surface seismic to borehole measurements. The upgoing waves are those reflected from interfaces and correspond to the reflections imaged with surface seismic. Figure 1b shows the crosswell geometry, which has borehole sources and borehole sensors. The crosswell survey has higher resolution (about 1-5 m) because the subsurface source allows higher frequency propagation over (typically) shorter distances than surface source data. However the crosswell is limited to the interwell volume while the VSP can potentially image on any azimuth. Crosswell acquisition allows tomographic imaging of seismic velocity between the boreholes.

Crosswell seismic methods have been successfully applied to CO2 injection monitoring, initially as part of enhanced oil recovery (EOR) (e.g. Harris et al.1995; Lazaratos and Marion 1997; Gritto et al. 2004) and more recently as part of a sequestration pilot test (Xue et al. 2005; Spetzler et al. 2006). These studies were successful in detecting changes in seismic velocity caused by CO_2 injection into reservoirs. In the case of oil reservoirs the interpretation can be more difficult because of multi phase fluids (e.g. methane, brine, oil and CO_2, as described in Hoversten et al. 2003). In sequestration pilots, the CO_2 is typically injected into brine aquifers (Arts et al. 2002; Xue et al. 2005). Xue et al. (2005) found a velocity reduction of about 3% from crosswell tomography and a reduction of up to 23% at the well bore via sonic logging. Arts et al. (2002) present surface seismic monitoring results that show reflection amplitude change in the CO2 injection volume. The VSP method is useful for interpreting surface seismic and was used in this way at the Weyburn field CO_2 EOR project (Majer et al. 2006).

The goals of the crosswell survey were to spatially map the CO_2 between the wells using P- and S-wave velocity tomographic imaging, and to use these properties to estimate the CO_2 saturation between the wells. The goals of the VSP were to spatially map the CO_2 beyond the well pair and to image nearby structures such as faults. The time-lapse VSP and crosswell surveys were acquired together, with pre-injection surveys in July 2004 and post-injection surveys in late November 2004, about 1.5 months after the CO_2 injection.

In the following sections we will describe the geologic background, the data acquisition and analysis, interpretation of the results and then give a summary and conclusions.

Site Background and Characterization

The Frio site was chosen for a small scale pilot test of CO_2 injection into a brine aquifer specifically to study sequestration issues. The pilot study had goals to safely inject anthropogenic CO_2, model the expected flow, sample the fluid in an up-dip observation well and monitor the resulting plume (Hovorka et al. 2006). The selection and characterization of the Frio site, along with stratigraphic figures, has been described in Hovorka et al. (2006) and in this issue (Doughty et al. 2006) and will be summarized here. The injection site was selected in 2003 after characterization of 21 representative saline formations in the onshore United States. The selected aquifer is part of the on-shore Gulf of Mexico Frio formation sandstone, near Houston, TX. The experimental site is in an oil field, where site access, use of an idle well as an observation well, wireline well logs, 3-D seismic, and production data were donated by the operator, Texas American Resources. A new well was drilled for injection about 30 m offset from the existing observation well. The CO_2 injection took place over 10 days in October 2004 with about 1600 tons of supercritical CO_2 injected into the upper C-sand of the Frio Formation at a depth of 1528.5 - 1534.7 m (5015 to 5030 ft). The downhole pressure was about 150 bars with about 2-3 bar variation during injection (Hovorka et al. 2006). The downhole temperature was about 55°C. At these conditions the CO_2 is in a supercritical liquid state with density of 653 kg/m3 and P-wave velocity of 335 m/s (National Institute of Standards and Technology 2006). The injected CO_2 is expected to displace the brine with some amount dissolving into the brine.

Sandstones of the Oligocene Frio Formation are a potential target for large-volume storage because they are part of a thick, regionally extensive sandstone trend that underlies a concentration of industrial sources and power plants along the Gulf Coast of the United States. Detailed characterization was conducted using traditional reservoir assessment tools. From this characterization, a numerical reservoir model was created using LBNL's TOUGH2 code (Pruess 2004; Doughty et al. 2006). Geologically constrained numerical models of injection and monitoring scenarios were prepared and used to optimize the experimental design, well locations and completion, and monitoring tool selection. The upper Frio in the study area is composed of northwest-southeast-elongated fluvial sandstone separated by mudstones and shales that can be correlated over the field but not regionally. The upper Frio “C,” “B,” and “A” (in lower to upper stratigraphic order) sandstones are part of a trend of fluvial sandstones that were increasingly reworked beneath the regionally extensive 60-m-thick (200-ft) shales and mudstones of the overlying Anahuac Formation. The selected injection zone, the upper half of the Frio “C” sandstone, is a 22.8-m (75-ft) upward-fining, fine-grained, poorly indurated, well-sorted sandstone. The upper part of the “C” sandstone has porosities of 30 to 35% and permeabilities of 2,000 to 2,500 md (Hovorka et al. 2006). The top “C” seal is composed of shale, sands, and siltstones that form a minor seal beneath the regional Anahuac Shale but probably a major barrier to vertical flow out of the “C” sandstone.

Structural analysis of the injection interval using logs and 3-D seismic shows that the upper Frio Formation at the test site is within a fault-bounded compartment that is part of a system of radial faults above a nearby salt dome. Dips within the injection compartment are steep. Hand-picked interpretation of the FMI (formation microimager) log by Schlumberger measured dips of 18 degrees to the south at the injection well; interwell correlation measured an average dip of 16 degrees south (Hovorka et al. 2006).

Seismic Data Acquisition

The data acquisition description is divided into sensors, sources and recording system. For sensors, both the VSP and crosswell surveys used an 80-level 3-component, clamping geophone string, which was supplied by Paulsson Geophysical and was deployed on special tubing. Each of the 80 3-component sensors was independently clamped to the borehole wall, allowing measurement of ground motion (velocity). The sensors were spaced every 7.6 m (25 ft) along the string, so the 80 sensors spanned 610 m (2000 ft) of the borehole. Figure 2 shows the deployment depths of the sensor string. The 3-component sensors allowed optimal measurement of compressional (P) and shear (S) waves, which are orthogonally polarized.

For the crosswell survey, the source was an orbital vibrator, supplied by LBNL The orbital vibrator source is an eccentric mass rotated by an electric motor. The source is wireline operated and fluid coupled to the surrounding formation. The rate of rotation is linearly varied from 0 to 350 Hz and back to stop. Useable energy is acquired above about 70 Hz, giving a 70 to 350 Hz bandwidth. At each source location a clockwise and counter clockwise sweep is recorded. Decomposition of these two sweeps provides two equivalent sources with orthogonal horizontal oscillations (Daley and Cox 2001). Component rotation using P-wave particle motion rotates these two sources into in-line and cross-line equivalents, with in-line being horizontal and in the plane of the two boreholes. This rotation results in a 6-component receiver gather with in-line and cross-line sources for the vertical and two horizontal receiver components. The in-line source generates predominantly P-wave energy while the cross-line source generates predominantly S-wave energy. Consistent generation of both P- and S-waves is a notable feature of the orbital vibrator source.

In the crosswell survey, both the source and receiver spacing was 1.5 m, with the sources spanning 75 m and the sensors spanning 300 m (only the deepest 40 of the 80 sensors were recorded in the crosswell survey). The sensor string was moved five times at 1.5 m intervals to give 1.5 m sensor spacing from the 7.6 m fixed spacing. Five source 'fans' (all source depths for each of 5 sensor string locations) were thus acquired in the crosswell survey. The survey was conducted using the injection well for sensors and the monitoring well for sources. Source and sensor locations were centered on the injection interval.

The VSP used the same 80 level, 3-component geophone string with explosive sources. The explosive shot holes were about 18 m (60 ft.) deep. A single shot with about 3.5 lbs of seismic explosive was recorded for each sensor string location at each shot point. Eight shot points were acquired (Figure 3). The sensors were interleaved to give spacings of 1.5 to 7.5 m (partially because of the needs of the crosswell recording). Smaller sensor spacing has the advantage of increasing spatial sampling and therefore increasing the spatial resolution of subsurface changes. The shotpoints were offset 100 to 1500 m from the sensor well. The locations of the VSP shotpoints were chosen to monitor the estimated CO_2 plume location (sites 1-4 in Figure 3) and to provide structural information at the injection site (sites 5-9 in Figure 3). Other sites were planned but not obtained due to permitting issues and local flooding. These sites (one to the Northeast and one to the South, would have allowed imaging to larger offsets (about 500 m) on these azimuths.

Data Processing and Analysis

The processing of the VSP focused on time lapse change in reflection amplitude of the reservoir horizon. Initial processing included applying time shifts to correct for shot variations (as measured with a surface geophone at each shot point), picking of arrival times at each depth, separation of down-going and up-going (reflected) wavefields, converting reflections to two-way travel time and enhancing the reflected energy signal using frequency-wavenumber filters. A description of these standard VSP processing details is given in Yilmaz (1987). Following these processing steps, an amplitude equalization was applied using a reflection above the reservoir (the ‘control’ reflection labeled in Figure 4. This equalization assumes that amplitude changes in a reflector are due to shallow sub-surface changes (such as soil moisture saturation) or changes in the seismic source amplitude. Therefore the amplitude change measured in the shallow reflector is subtracted from all the data. Following this equalization, the time-lapse change in the reservoir reflection can be analyzed. The result from source site 1 is shown in Figure 4 where we see a clear increase in the reflection strength from the Frio formation. Similar results have been found from the sites 2, 3 and 4. For the VSP geometry, the reflection recorded at each sensor in the well originates at a different reflection point, so we are able to estimate the variation in reflection strength with offset along the azimuth between source and borehole. The VSP reflection change along three azimuths has been spatially mapped using ray tracing (similar to Figure 1a) to give an estimate of the reflection point location. Comparison of the VSP result with numerical modeling of CO_2 saturation will be discussed in the following interpretation section.

Before tomographic imaging, the travel times for P- and S-waves are determined. Typically the data is sorted into different ‘gathers’ with a common source depth, common sensor depth, or common source-sensor vertical offset. An example common offset gather of seismograms in Figure 5 shows good quality P- and S-wave direct arrivals, allowing velocity tomography. The travel times were picked manually using the in-line source and in-line sensor for P-wave and the cross-line source and cross-line sensor for S-wave. During the post-injection travel time picking, a large change in waveforms was observed in the injection zone (seen in Figure 5). This change was interpreted as 'guided waves' generated by a newly formed (and CO_2 induced) seismic low-velocity zone. Because guided waves do not follow the ray-theory used in standard tomographic inversion, travel times within the guided-wave zone were not used for inversion of time-lapse changes. Using the remaining picked travel times, tomographic imaging of velocity was performed.

The tomography processing had the following details: limited ray angles (no vertical offsets greater than 100 m), correction for the deviation of the boreholes from vertical (about 3-5 m of lateral offset), a straight ray projection, and a static correction to allow for borehole effects. Importantly, the data were inverted for the change in velocity, rather than inverting for each velocity field and then differencing. In this method the data input to the tomographic inversion is the travel time difference (postinjection time minus preinjection time) for each source-receiver pair. Typically, time-lapse tomography is done by computing two tomographic inversions with each travel time data set (the preinjection and the post injection) separately input to the tomographic inversion. By inverting the difference data, some potential errors (such as source and sensor locations) are minimized or eliminated (Ajo-Franklin et al. 2006; Spetzler 2006). The inversion algorithm is an algebraic reconstruction as described in Peterson et al. (1985). The inversion used a 2 m x 2m pixel size, with plotting interpolated to 0.5 m. The maximum spatial resolution is thus about 2m. Figure 6 shows the tomographic image of P- and S-wave velocity change. The P-wave tomogram shows a clear zone of change in the injection interval with P-wave velocity decreasing over 500 m/s in some pixels. The S-wave tomogram shows only small changes except for a small region near the injection zone where the S-wave velocity is reduced by up to 200 m/s.

Figure 7 shows a more detailed view of the P-wave velocity change within the injection zone, along with the well logs indicating CO_2 saturation near the boreholes. The well logs are Schlumberger's reservoir saturation tool (RST) (Adolph, et al., 1994). The CO_2 plume is clearly imaged by the velocity change, and the spatial agreement between the well logs and the tomograms provides mutual corroboration to each of these two independent measures of CO_2. Several attributes of the CO_2 induced change in seismic velocity can be observed via the tomogram and will be discussed in the interpretation section.

Interpretation

The injection of CO_2 causes a fluid substitution within the pore space. For fluid substitution with no change in matrix properties, a change in P-wave velocity is expected due to the change in bulk modulus (compressibility) with a minimal change in S-wave velocity expected due to the lack of change in shear modulus (which is a property of the rock matrix and not affected by pore fluid). Time-lapse tomographic imaging did map changes in P-wave velocity (over 500 m/s) due to the CO_2 plume (Figure 7). The S-wave velocity decrease near the injection well implies that there was some change in rock matrix properties (the shear modulus) in the near well region which was induced by the CO_2 injection. Overall, the lack of S-wave change confirms that the observed P-wave change is caused by fluid substitution of CO_2 for brine. The small change in pressure (about 3 bars) has a very minimal effect on velocity (about 1-10 m/s) due to the effective stress change. We can therefore interpret the following observations of velocity change in terms of CO_2 saturation. 1) The velocity change follows the dip of the stratigraphy. This observation is expected for CO_2 with buoyancy causing up-dip migration. 2) The velocity change is not homogeneous between the wells, with a larger change, and therefore a larger residual CO_2 saturation, in the downdip half of the tomogram. 3) The velocity change does not reach the actual top of the C-sand, which is in agreement with observed permeability reduction near the top of the sand. 4) The velocity change on the right half of the tomogram is somewhat layered with a larger change in the lower part (about 3 m thick) of the plume. This observation implies that the lower part of the plume has higher saturations, presumably due to the presence of a low permeability zone in the center or upper part of the plume.

Quantitative estimation of CO_2 saturation (the fractional part of the pore space filled with CO_2) from the change in seismic velocity is an ultimate goal, and such estimates can be obtained using a rock physics model. For our site, core studies typically used to build a rock physics model have not yet been performed and the unconsolidated sand limited core recovery. Similarly, well log measurement of seismic velocity, which could be closely tied to well log estimates of saturation (the RST log), failed to give useable results for post-injection in the injection zone. Nonetheless, quantitative CO_2 saturation estimates from seismic measurements using a rock physics model allow estimation of saturation in the interwell volume. Without site specific calibration we use results from similar high porosity sands such as used in Carcione et al. (2006). The resulting uncertainty is difficult to quantify but is probably in the range of 10% in saturation (based on variation with model parameters). We have built a rock physics model using recent work of Hoversten et al. (2003) with data from Carcione et al. (2006) (using the Utsira sand) and a model of fluid mixing proposed by Brie et al. (1995) to estimate the CO saturation from the seismic velocity. The CO_2 saturation is shown in Figure 8 where see saturations are estimated at about 20% in the region near the injection well and decrease to about 10% or less near the monitoring well. The CO_2 plume is about 5 m thick with the highest saturations (up to 20%) extending 15 m from the injection well. The lower half of the plume has higher concentrations, implying vertical heterogeneity (variation in permeability or porosity). The vertical variation is at the limit of the tomographic resolution (2 m), so greater detailed interpretation of the vertical heterogeneity is not possible. The saturation values are less than those observed in the RST, although the RST is a near-borehole measurement, not necessarily representative of the interwell region, and the RST had calibration problems for measurements made after the seismic surveys (Hovorka et al. 2006).

Interpretation of the VSP is focused on the large change in reflection amplitude and calculating this change as a function of offset from the injection well along each azimuth of a VSP source. Because we do not have an estimate of saturation directly from reflection strength, we compare the VSP result to the numerical model estimate of saturation. Figure 9 shows the offset dependent reflection change for a single azimuth with a comparison to the CO_2 saturation estimated at the same offset and azimuth using the TOUGH2 numerical flow model to estimate the spatial distribution of CO_2 saturation

(Doughty et al. this issue). We see a good qualitative agreement of the plume extent, about 80 m radially. Figure 10 shows this same comparison on three azimuths, North, Northwest and Northeast. We see the agreement is good to the North, moderate to the Northeast and worse to the Northwest. Since the numerical model is laterally and azimuthally homogeneous (allowing for formation dip), the disagreement indicates lateral heterogeneity imaged by the VSP which is not captured in the model.

The large VSP reflection response was somewhat unexpected because of the thinness of the CO_2 plume (about 5-7 m thick at 1500 m depth), and uncertainty in the expected velocity change. To verify the VSP result is consistent with the velocity change measured in the crosswell survey, we developed a numerical seismic model. The modeling used a 2-D elastic, finite-difference wave propagation code on a 201 by 652 grid with 5 m grid points (1 km by 3.3 km) and a 30 Hz center frequency. The initial 2-D velocity structure was built using horizons mapped from previous surface seismic, velocities measured by the pre-injection VSP, and velocity and density measured by pre-injection well logs. VSP data was generated using this pre-injection model. Two 'post-injection' VSP data sets were then calculated. The 'time-lapse' VSP response was calculated using the same processing as the field data, with the exception of amplitude calibration to a shallower reflection, which is unnecessary for numerical data with no shallow changes.

To obtain the post-injection model, we first applied the change in velocity, as mapped by the crosswell tomogram, to the 30 m wide zone between wells. This result underestimated the reflection amplitude change measured by the VSP. We then extended the velocity change beyond the wells using a 400 m/s velocity decrease (typical of that seen in the crosswell tomogram) applied to a 4 m thick zone over the horizontal distance predicted to contain CO_2 by the numerical flow modeling. This result overestimated the reflection amplitude change. These two modeled time-lapse VSP responses are shown in Figure 11, where we see that they bound the field measurement. This result demonstrates that velocity changes, on the order of those imaged by crosswell tomography, when they are extended beyond the interwell region, are able to generate the large reflection amplitude change observed in the VSP.

Conclusions

Sixteen hundred tons of CO_2 were injected into a brine aquifer at a depth of 1500 m at the Frio pilot site. Borehole seismic data, both VSP and crosswell, were acquired. Analysis of these time-lapse surveys provided in-situ estimates of the spatial distribution of injected CO_2, with high resolution tomographic imaging between injection and monitoring wells (crosswell), and lower resolution VSP reflection imaging at larger distances, on different azimuths. The crosswell tomogram shows seismic P-wave velocity decreases up to 500 m/s, while the S-wave velocity shows minimal change. The spatial change in P-wave velocity can be interpreted for details of the CO_2 saturation distribution, including buoyant up-dip flow with some layering and less change in velocity on the up-dip half of the tomogram, indicating permeability heterogeneity. Initial development of a rock physics model allows estimates of CO_2 saturation between the wells from the crosswell tomogram. The VSP results, using changes in reflection amplitude from the injection horizon, show a large increase (up to 70%) and show azimuthal variation, also indicating CO_2 flow heterogeneity. Numerical modeling of the VSP response uses the crosswell measurements to show that velocity changes seen in the interwell volume can cause the large response in the VSP reflectivity change if the velocity change is extended beyond the wells. It is reasonable to infer that the large reflection response seen in the VSP would allow surface seismic monitoring of similar CO_2 plumes, allowing monitoring of small plumes away from boreholes. This result demonstrates that small CO_2 plumes (such as those migrating away from a major injection) are detectable in saline aquifers.

Acknowledgments:

This work was supported by the GEOSEQ project for the Assistant Secretary for Fossil Energy, Office of Coal and Power Systems through the National Energy Technology Laboratory, of the US Department of Energy, under Contract No.DE-AC02-05CH11231. The CO2 flow modeling results were prepared by Chris Doughty of LBNL. Thanks to Susan Hovorka and Sally Benson for management of the Frio and GEOSEQ projects, respectively, and their support of the geophysics program. Thanks to Don Lippert, Cecil Hoffpauir and Rob Trautz for their important contributions to the data acquisition.

Thanks to Bjorn Paulsson of P/GSI . Thanks to the editors and anonymous reviewers for helpful comments and corrections.

References:

Adolph B, Stoller C., Brady J., Flaum C., Melcher C,. Roscoe B., Vittachi A. (1994) Saturation monitoring with the RST Reservoir Saturation Tool. Oilfield Review 6:29-38.

Ajo-Franklin J.B., Urban J, Harris J.M. (2006) Temporal Integration of Seismic Traveltime Tomography. Society of Exploration Geophysicists Annual Meeting, Expanded Abstracts 25:2468.

Arts R., Elsayed R., Van Der Meer L., Eiken O., Ostmo O., Chadwick A., Kirby G. and Zinszner B. (2002) Estimation of the Mass of Injected CO_2 at Sleipner Using Time-Lapse Seismic Data. paper H-16, EAGE 64th Annual Conference.

Balch A.H. and Lee M.W., (ed) (1984) Vertical Seismic Profiling: Technique, Applications, and Case Histories. International Human Resources Development Corporation, Boston, MA.

Brie A., Pampuri F., Marsala A.F., and Meazza O. (1995) Shear sonic interpretation in gas-bearing sands. SPE Annual Technical Conf., 30595:701-710.

Carcione J.M., Picotti S., Gei D., Rossi G. (2006) Physics and Seismic Modeling for Monitoring CO_2 Storage. Pure and Applied Geophysics 163:175 – 207 DOI 10.1007/s00024-005-0002-1.

Daley T.M. and Cox D. (2001) Orbital vibrator seismic source for simultaneous P- and S-wave crosswell acquisition. Geophysics 66:1471-1480.

Gritto R., T.M. Daley and L.R. Myer (2004) Joint cross-well and single-well seismic studies at Lost Hills, California. Geophysical Prospecting 52:323-339

Hardage B.A. (2000) Vertical Seismic Profiling: Principles, Handbook of Geophysical Exploration: Seismic Exploration, 14, Elsevier.

Harris J.M., Nolen-Hoeksema R.C., Langan R.T., Van Schaack M., Lazaratos S.K., Rector J.W. (1995) High-resolution crosswell imaging of a west Texas carbonate reservoir: Part1-Project summary and interpretation. Geophysics 60:667-681.

Hoversten G., M., Gritto R., Washbourne J., Daley T. M, (2003) Pressure and Fluid Saturation Prediction in a Multicomponent Reservoir, using Combined Seismic and Electromagnetic Imaging. Geophysics 68:1580-1591.

Hovorka S.D., Benson S.M., Doughty C., Friefeld B.M., Sakurai S., Daley T.M. (2006) Measuring permanence of CO2 storage in saline formations: the Frio experiment. Environmental Geosciences 13:1-17 DOI:10.1306/eg.11210505011

Lazaratos S.K., and Marion B.P. (1997) Crosswell seismic imaging of reservoir changes caused by CO2 injection. The Leading Edge 16:1300-1306.

Majer E.L., Daley T.M., Korneev V., Cox D., Peterson J.E. (2006) Cost-effective imaging of CO2 injection with borehole seismic methods. The Leading Edge, 25, p1290.

National Institute of Standards and Technology (2006), Thermophysical Properties of Carbon Dioxide. http://webbook.nist.gov/cgi/fluid.cgi?ID=C124389&Action=Page Cited Nov 17, 2006.

Pacala S., and Socolow R. (2004) Stabilization Wedges: Solving the Climate Problem for the Next 50 Years with Current Technologies. Science 305:968-972.

Peterson, J.E. Paulsson B.N. and McEvilly T.V. (1985) Applications of algebraic reconstruction techniques to crosshole seismic data. Geophysics 50:1566-1580.

Pruess K. (2004) The TOUGH Codes - A Family of Simulation Tools for Multiphase Flow and Transport Processes in Permeable Media. Vadose Zone Journal 3:738-746.

Spetzler J., (2006) Time-Lapse Seismic Crosswell Monitoring of Steam Injection in Tar Sand, Society of Exploration Geophysicists Annual Meeting, Expanded Abstracts v25, p3120.

Spetzler J., Xue Z., Saito H., Nobuoka D., Hiroyuki A., Nishizawa O. (2006) Time-Lapse Seismic Crosswell Monitoring of Co2 injected in an Onshore Sandstone Aquifer. Society of Exploration Geophysicists Annual Meeting, Expanded Abstracts 25:3285.

Yilmaz O. (1981) Seismic Data Processing. Investigations in Geophysics no. 2, Society of Explorations Geophysicists.

Xue Z., Tanase D., Saito H., Nobuoka D., Watanabe J (2005) Time-lapse crosswell seismic tomography and well logging to monitor the injected CO2 in an onshore aquifer. Nagaoka, Japan, Society of Exploration Geophysicists Annual Meeting, Expanded Abstracts 24:1433.

Figure Captions:

Figure 1a (left) Schematic of VSP data acquisition with direct raypaths (yellow), reflected raypaths (blue), and boreholes (yellow and purple vertical lines)

1b) (right) Schematic of crosswell acquisition with sensors (green) and sources (red) in separate boreholes (yellow and purple) with raypaths in yellow.

Figure 2. Sensor string deployment depths with each line segment representing one deployment. FFID is the field file identification number. For the crosswell deployments only the bottom half of the sensors were recorded.

Figure 3. VSP shot point locations along with the two wells (in light blue).

Figure 4. VSP reflection amplitude comparison. A large increase in amplitude is observed for the Frio reflection. The control reflection is the one used for amplitude normalization between surveys.

Figure 5. Comparison of zero-offset gathers from the crosswell survey. A decrease in travel time within the injection zone can be observed.

Figure 6. Tomographic image of P-wave velocity change (left) and S-wave velocity change (right) from the crosswell survey.

Figure 7. Detailed view of the injection region of the P-wave tomogram along with RST logs for each well. The RST log had multiple runs with the change shown in yellow.

Figure 8. CO2 saturation estimated from the P-wave velocity change using a rock physics model.

Figure 9. VSP reflection amplitude change compared with CO2 saturation estimated by flow modeling, as a function of offset from the injection well on the Northern azimuth.

Figure 10 VSP reflection amplitude change compared with CO2 saturation estimated by flow modeling, as a function of offset from the injection well on three azimuths.

Figure 11. Numerical modeling of VSP reflection amplitude change compared to field data. The model using the predicted plume extent extendes the velocity change over more than 130 m laterally, While the variable change model only had velocity change between the wells (about 30 m).

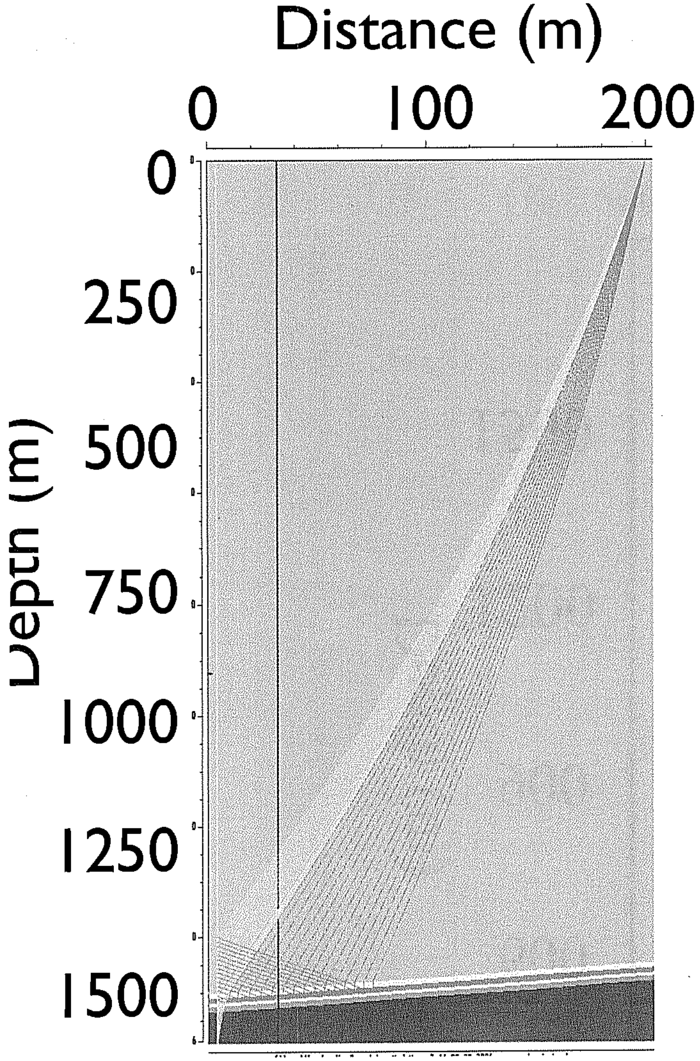

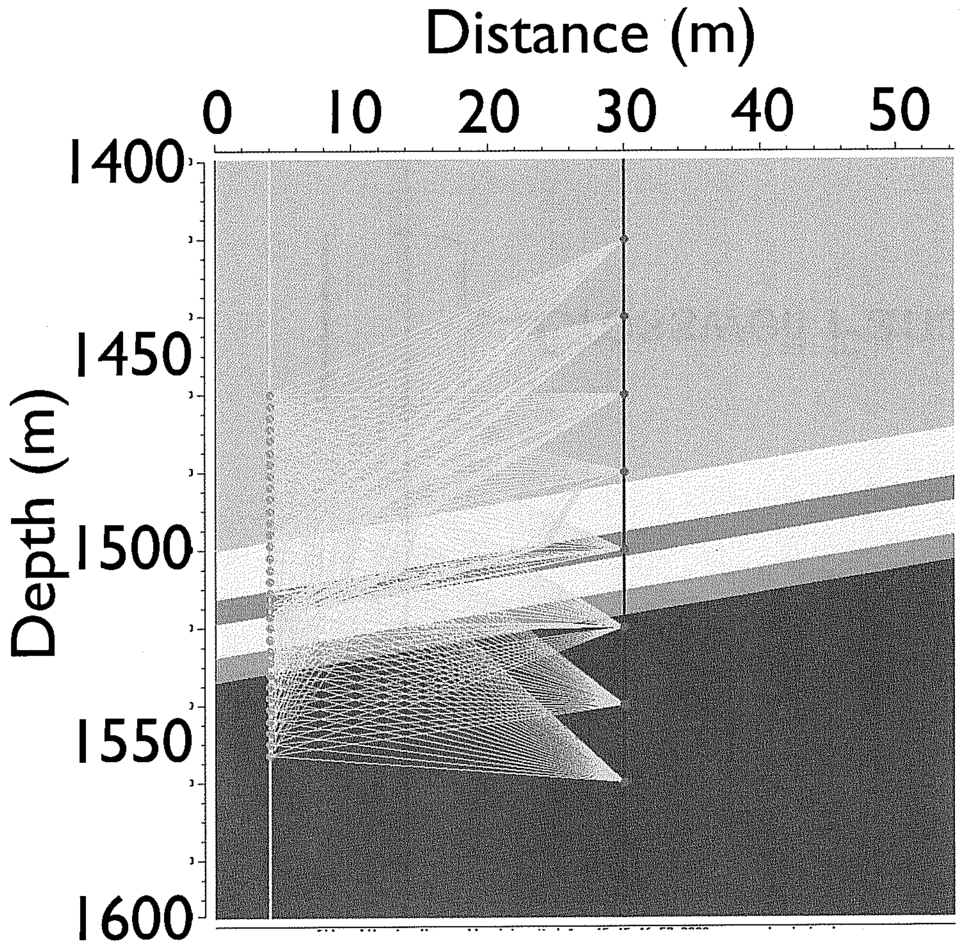

Figure 1a (left) Schematic of VSP data acquisition with direct raypaths (yellow), reflected raypaths (blue), and boreholes (yellow and purple vertical lines)
1b) (right) Schematic of crosswell acquisition with sensors (green) and sources (red) in separate boreholes (yellow and purple) with raypaths in yellow.

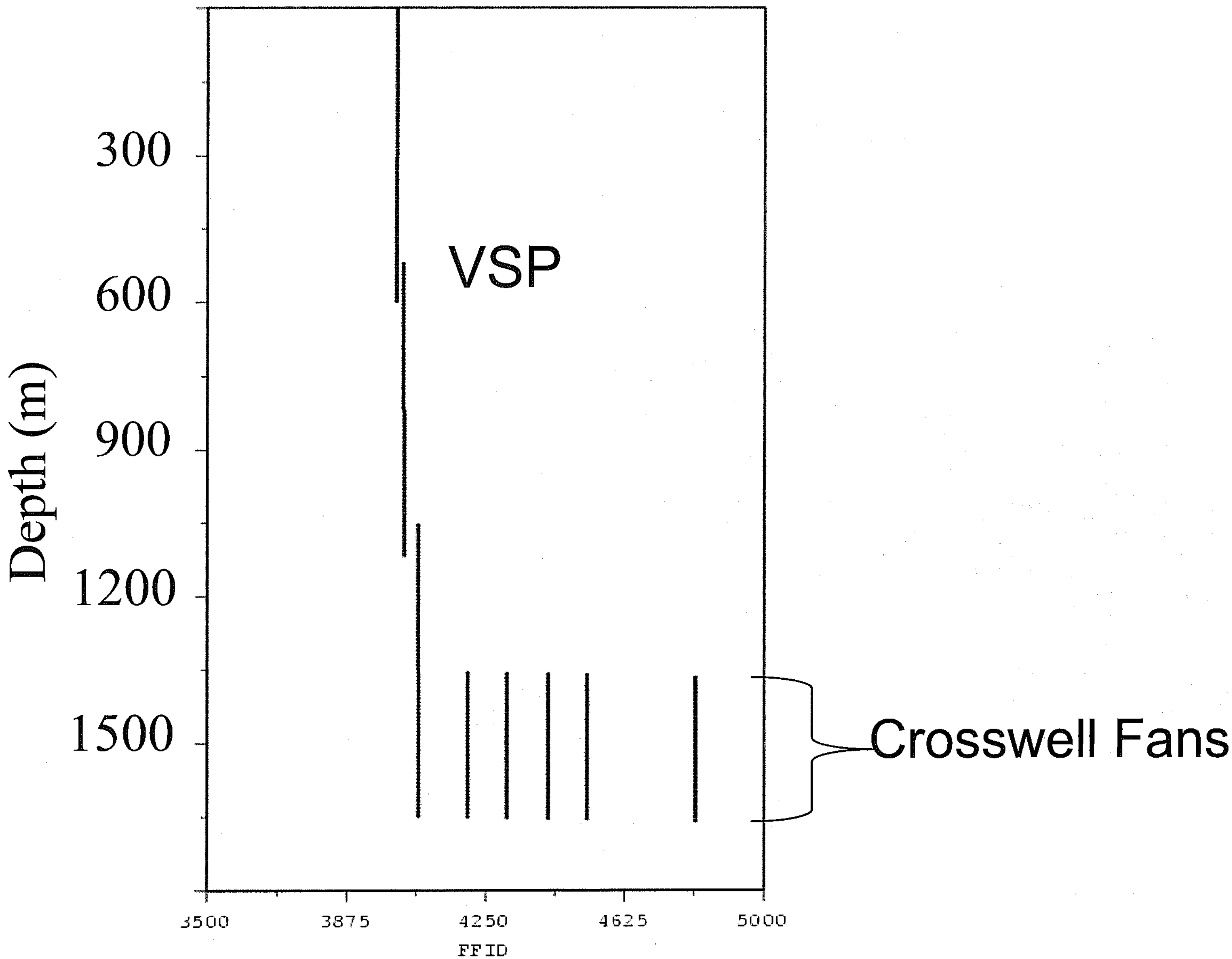

Figure 2. Sensor string deployment depths with each line segment representing one deployment. FFID is the field file identification number. For the crosswell deployments only the bottom half of the

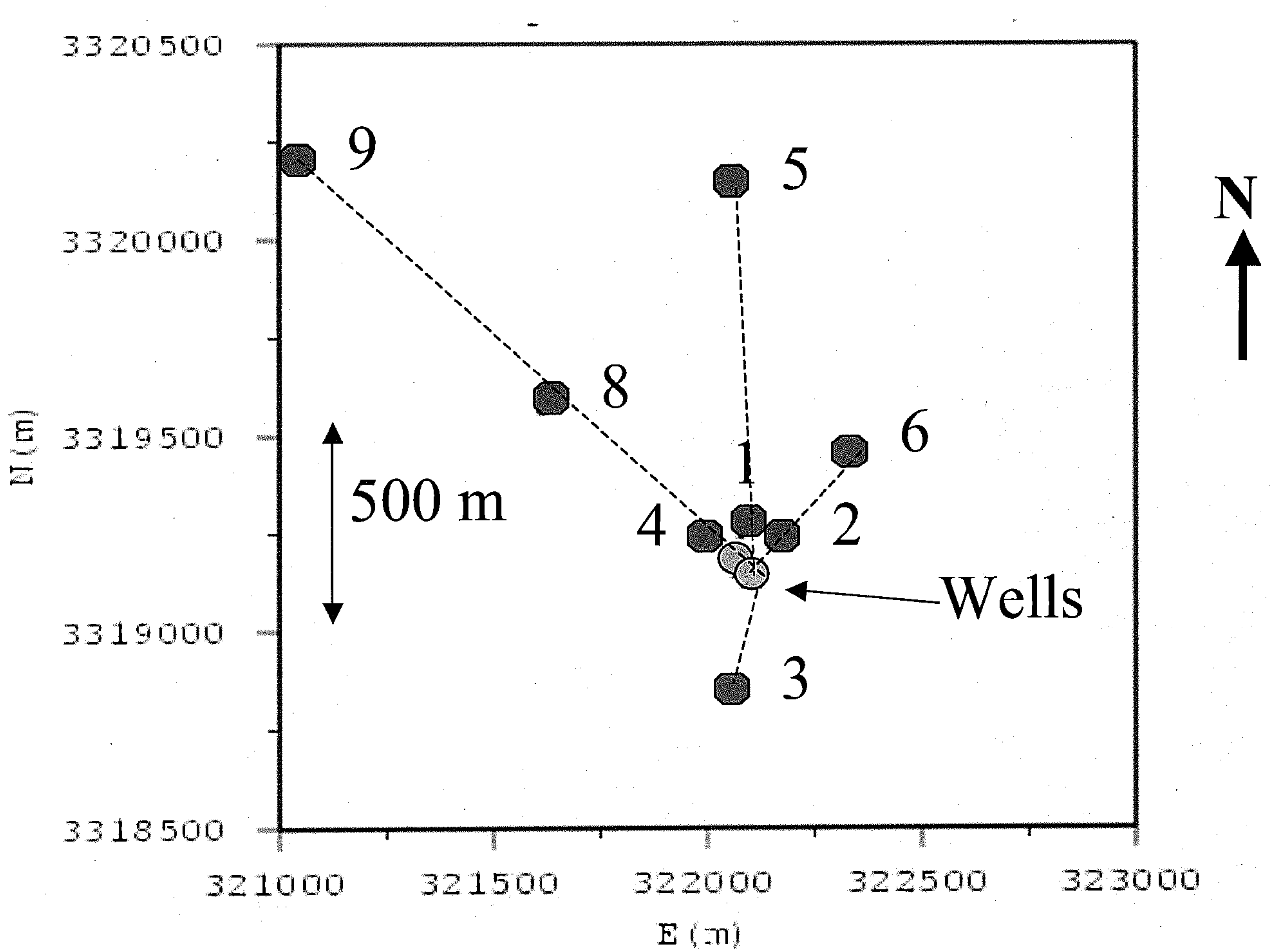

Figure 3. VSP shot point locations along with the two wells (in light blue).

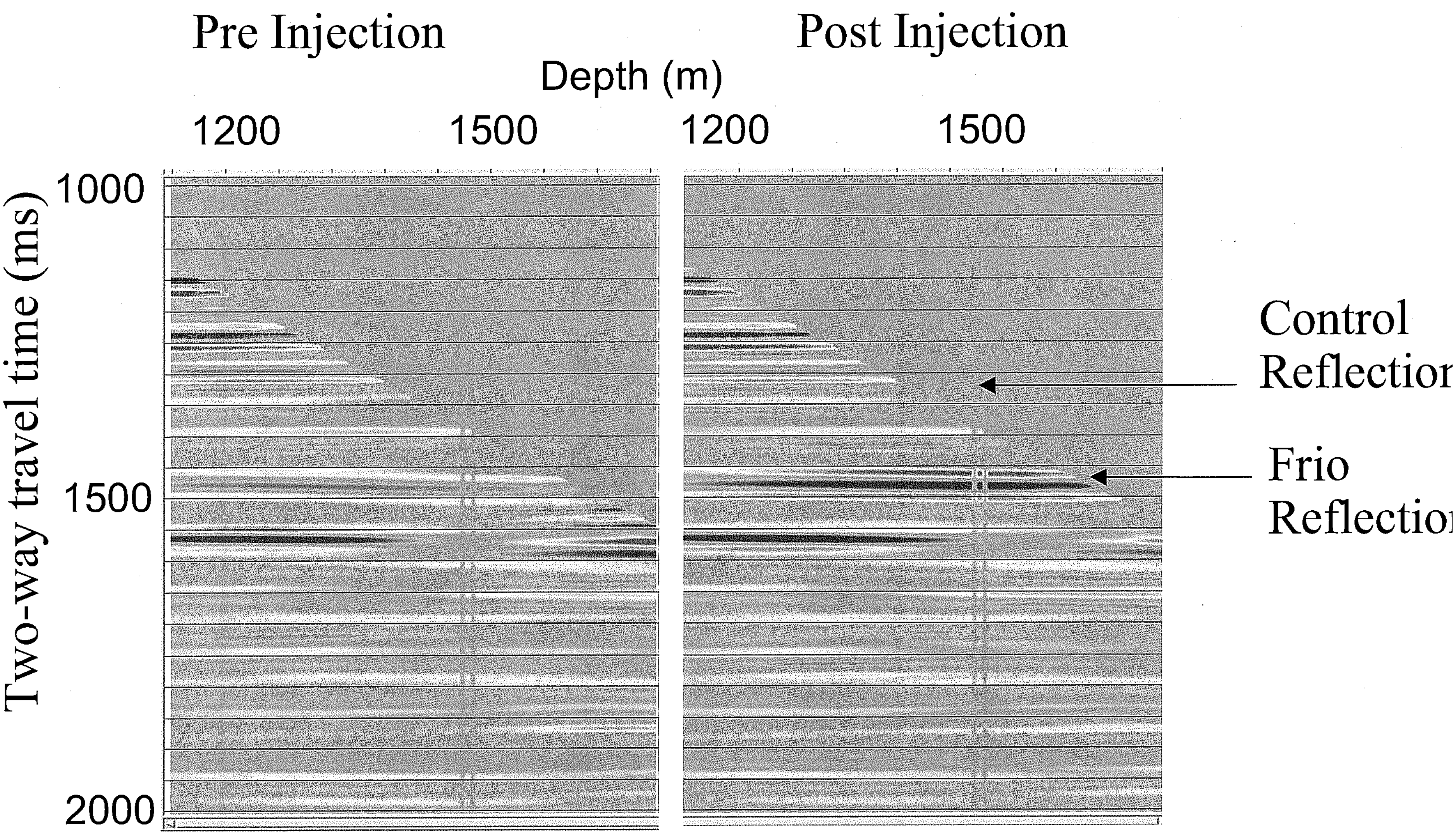

Figure 4. VSP reflection amplitude comparison. A large increase in amplitude is observed for the Frio reflection. The control reflection is the one used for amplitude normalization between surveys.

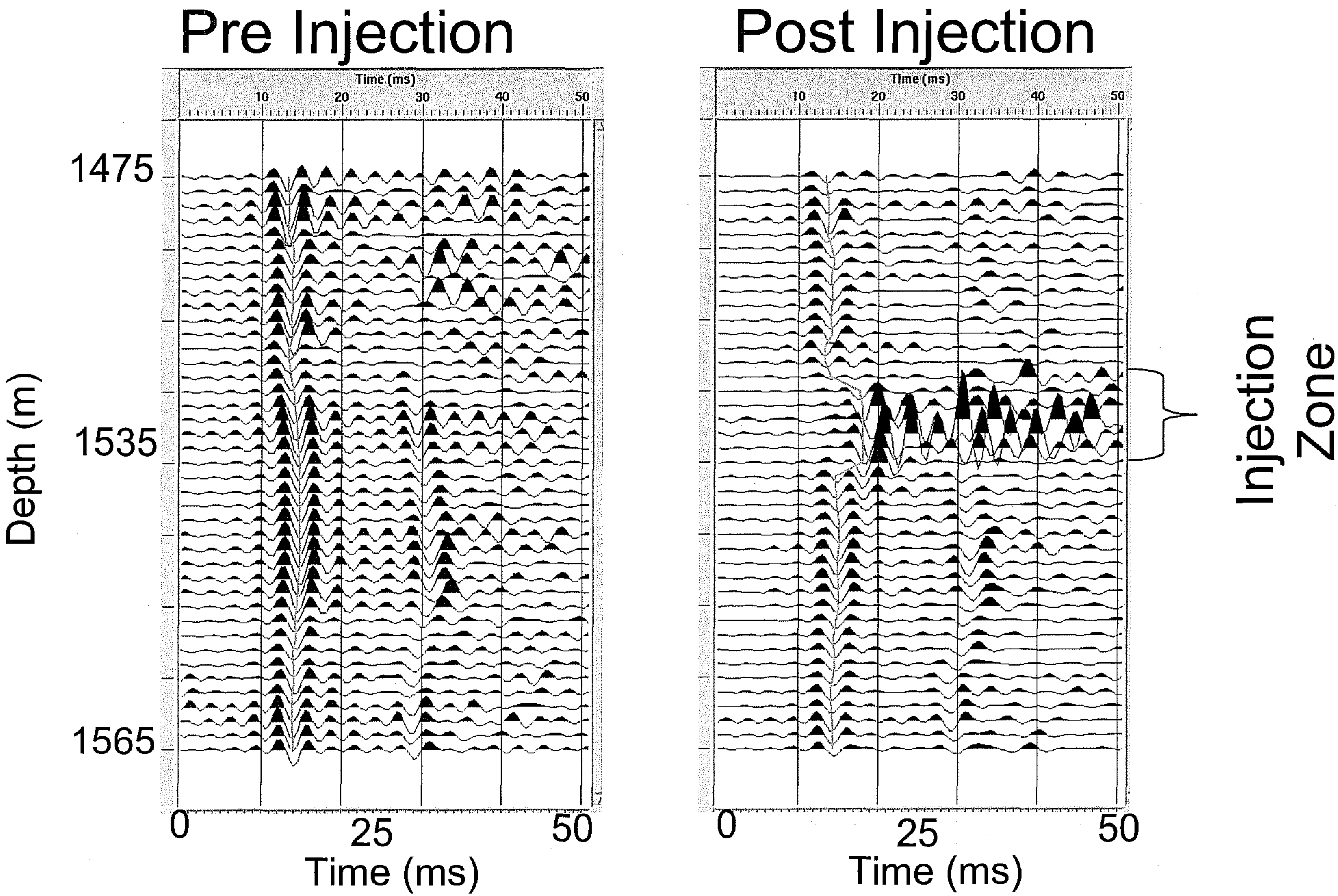

Figure 5. Comparison of zero-offset gathers from the crosswell survey.
A decrease in travel time within the injection zone can be observed.

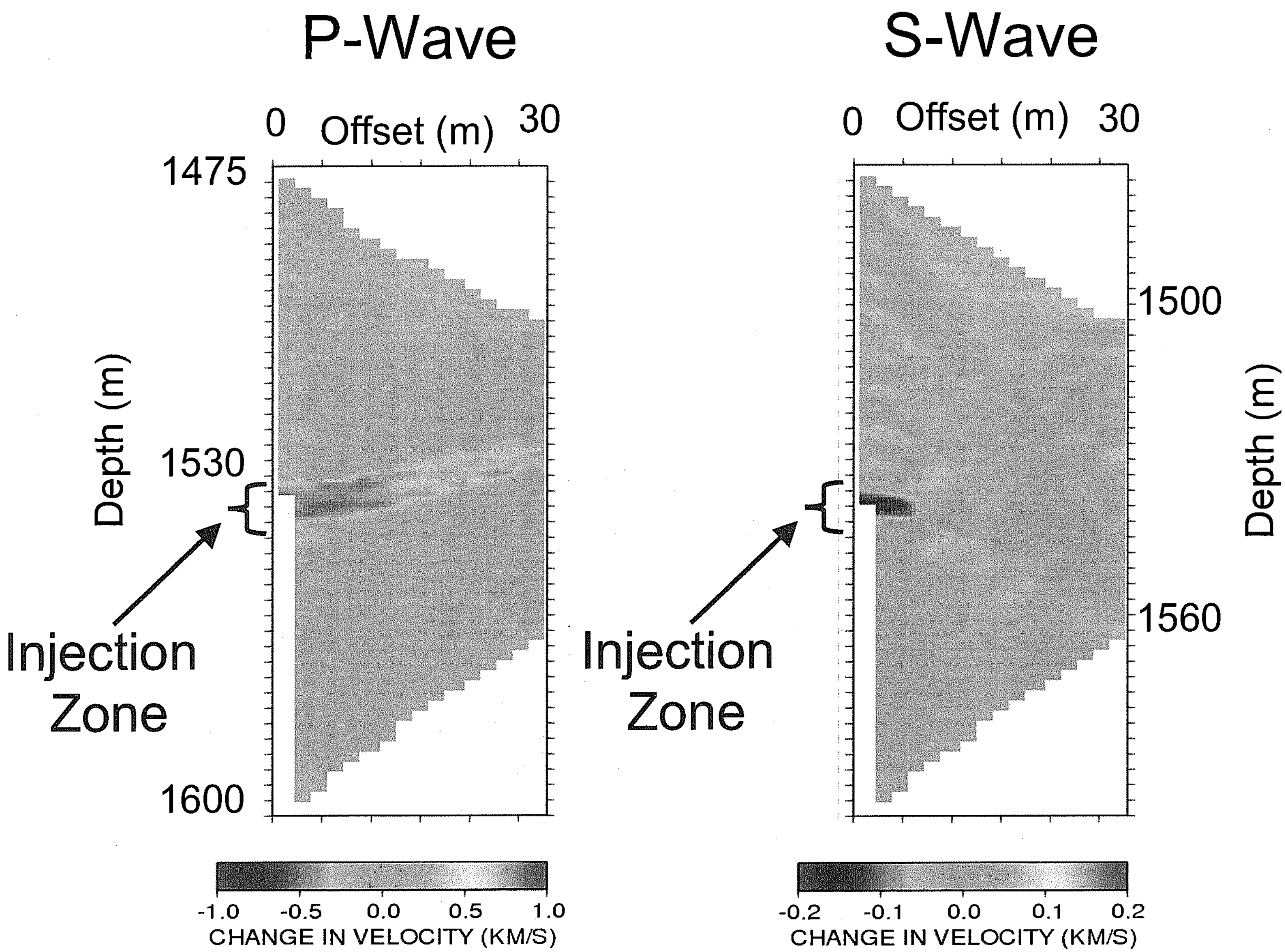

Figure 6. Tomographic image of P-wave velocity change (left) and S-wave velocity change (right) from the crosswell survey.

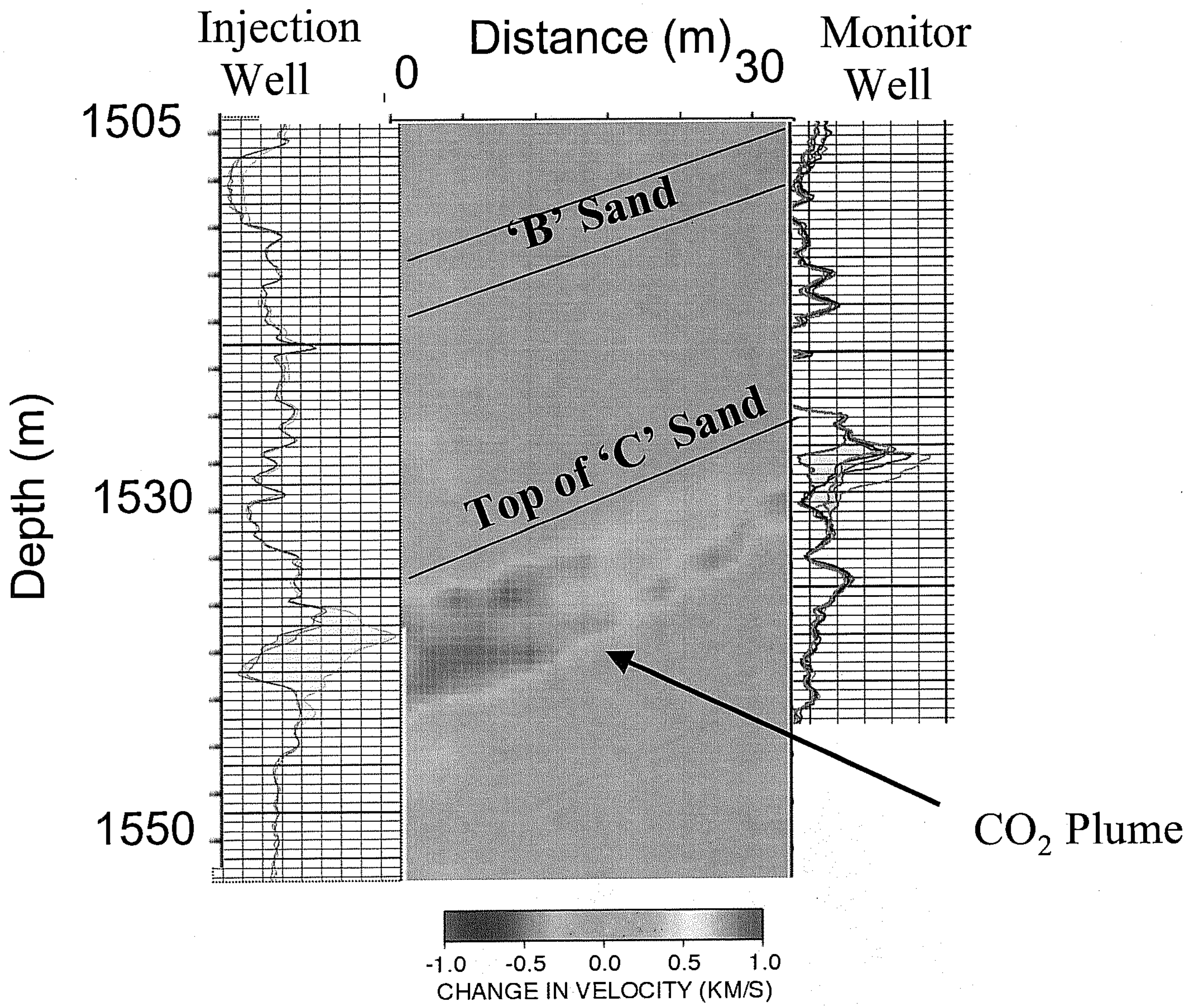

Figure 7. Detailed view of the injection region of the P-wave tomogram along with RST logs for each well. The RST log had multiple runs with the change shown in yellow.

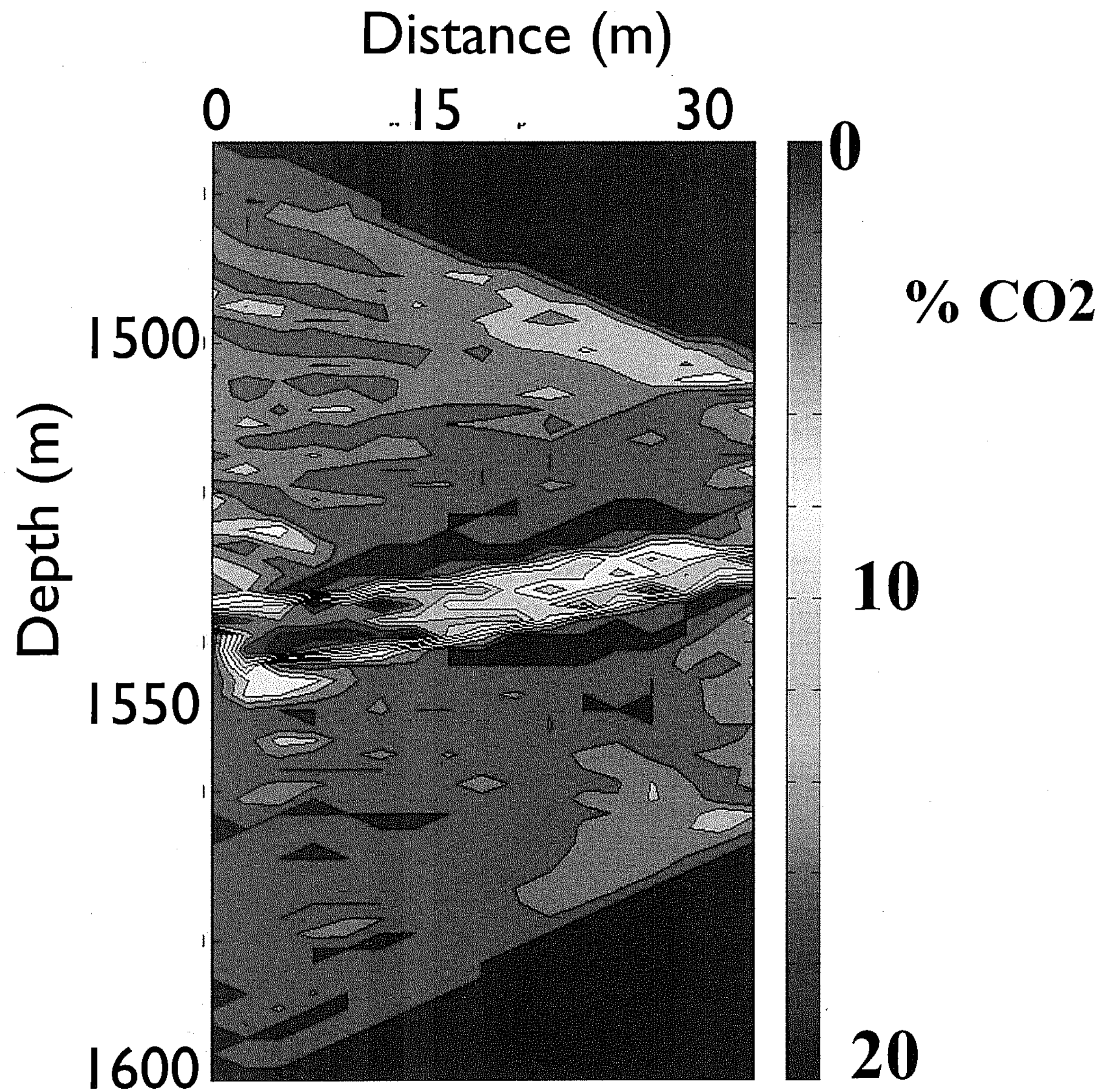

Figure 8. CO2 saturation estimated from the P-wave velocity change using a rock physics model.

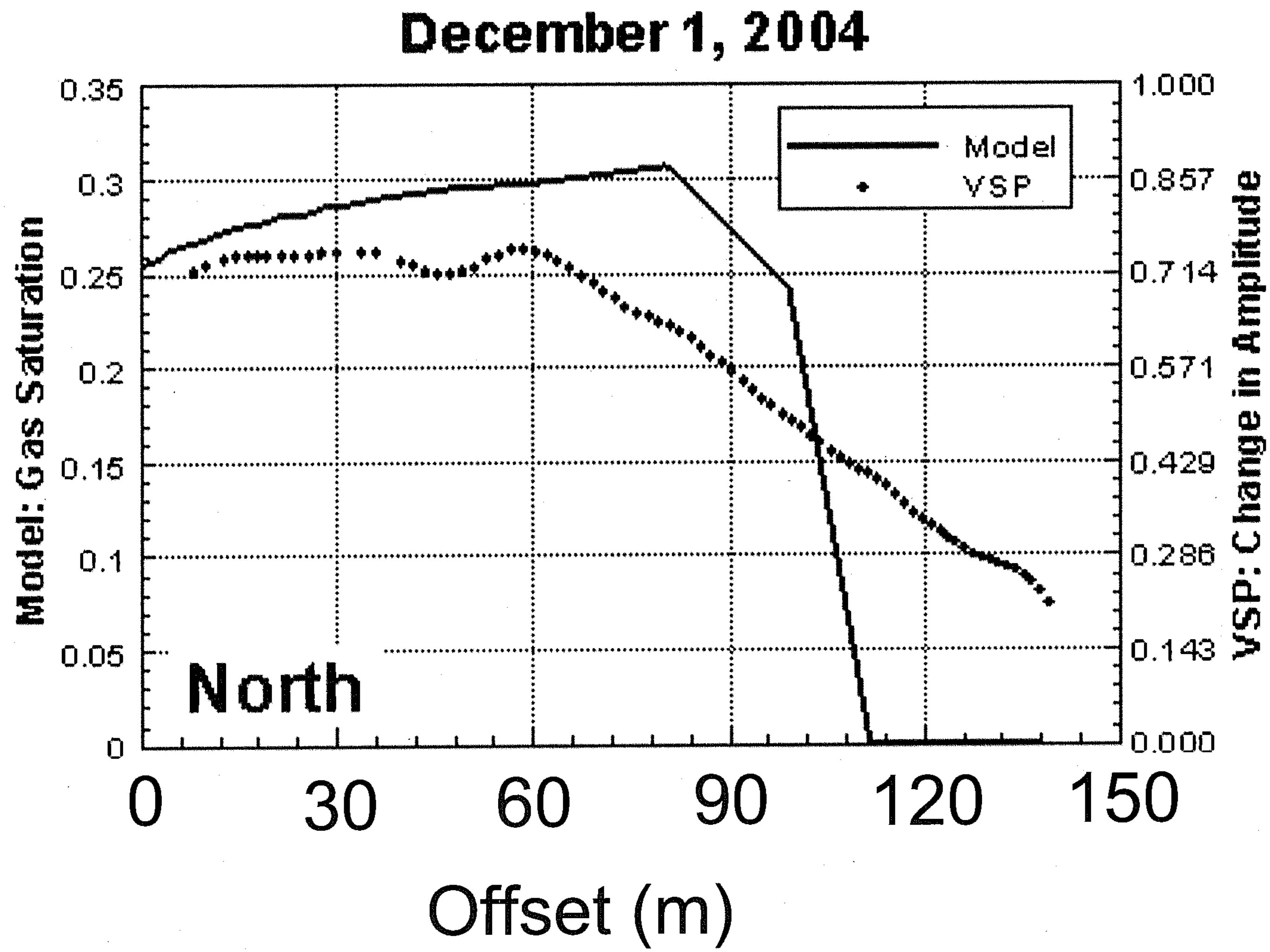

Figure 9. VSP reflection amplitude change compared with CO2 saturation estimated by flow modeling, as a function of offset from the injection well on the Northern azimuth.

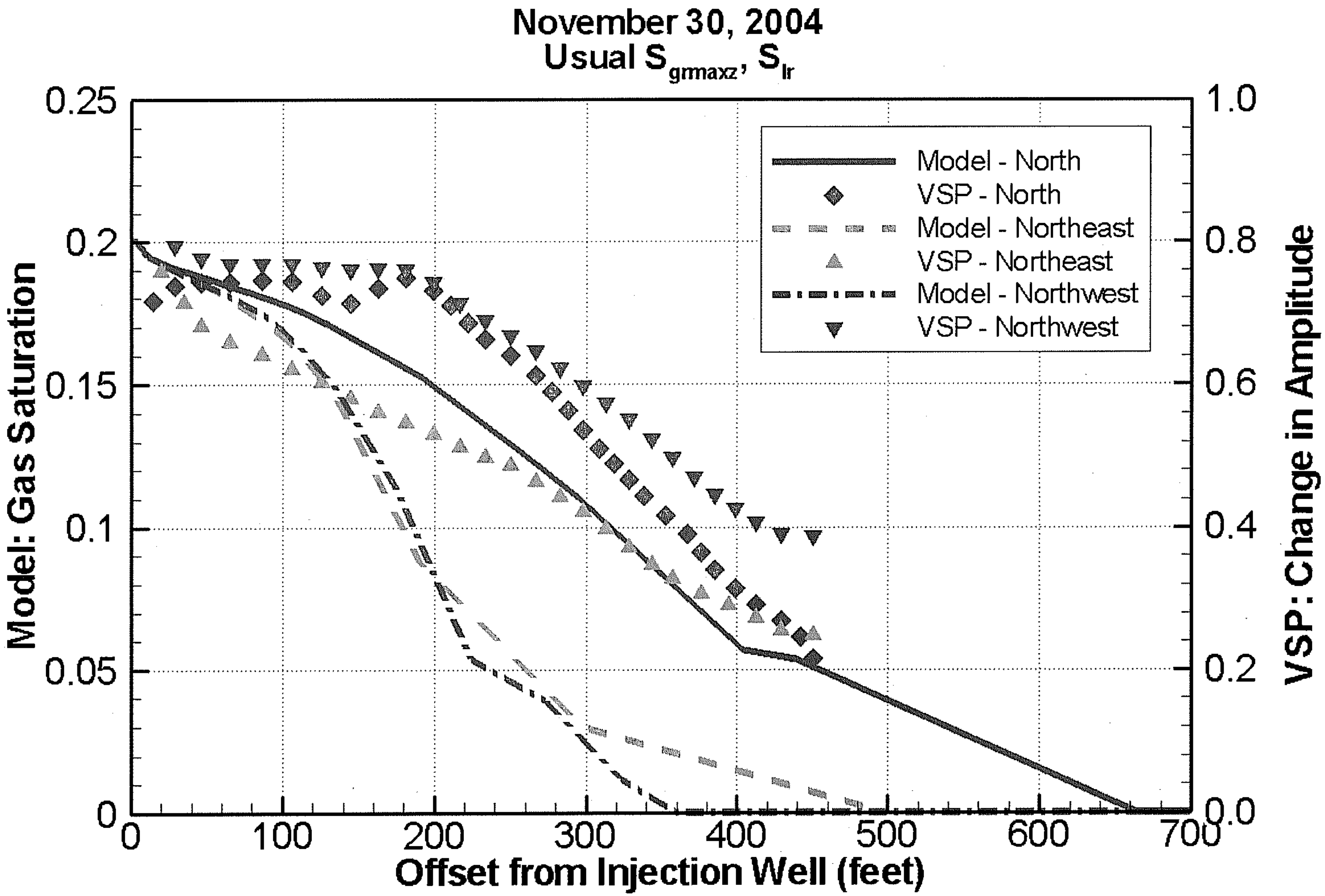

Figure 10 VSP reflection amplitude change compared with CO2 saturation estimated by flow modeling, as a function of offset from the injection well on three azimuths.

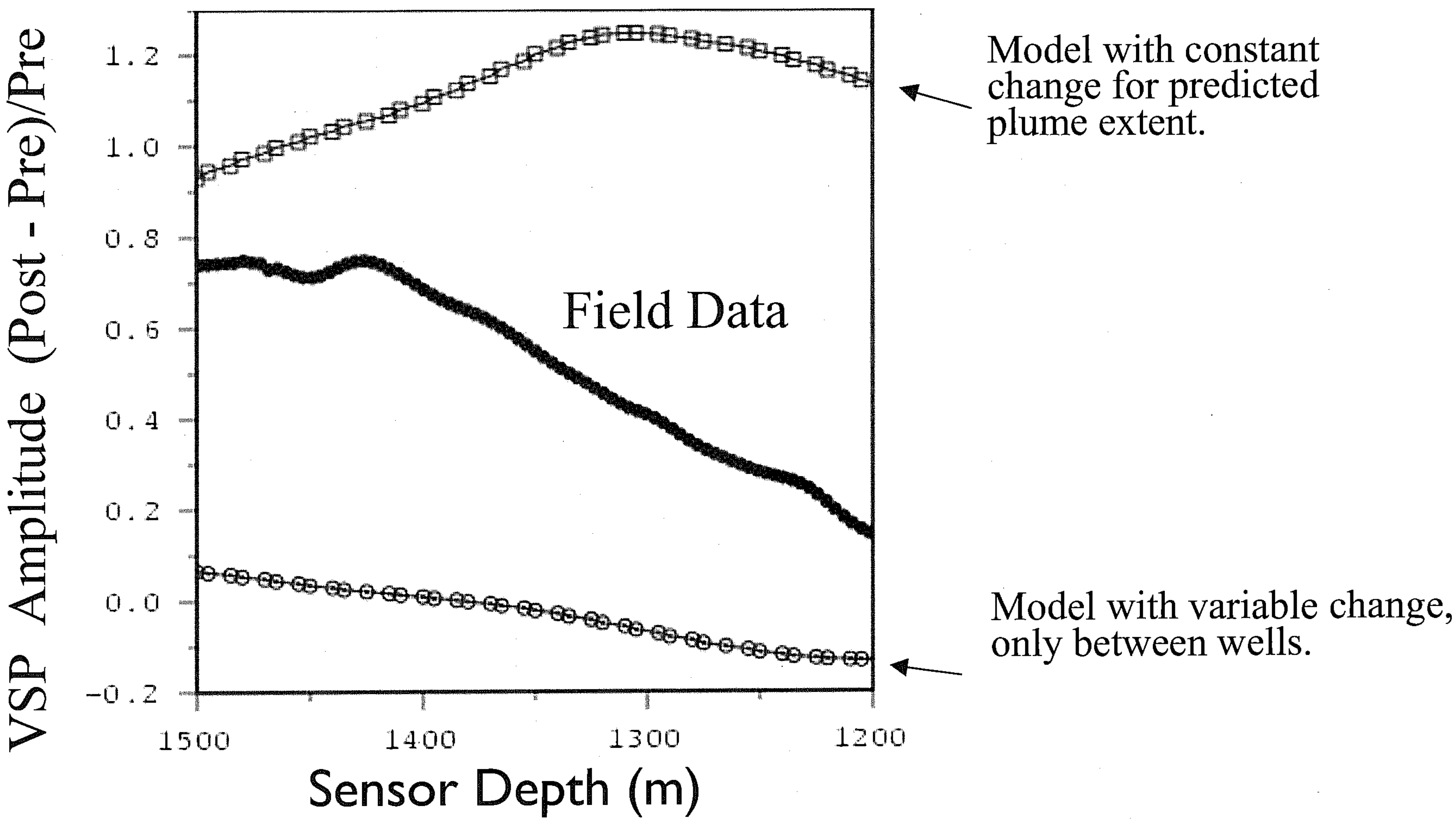

Figure 11. Numerical modeling of VSP reflection amplitude change compared to field data. The model using the predicted plume extent extendes the velocity change over more than 130 m laterally, While the variable change model only had velocity change between the wells (about 30 m).